NeuroImage 332 (2026) 121903

Contents lists available at ScienceDirect

NeuroImage

journal homepage: www.elsevier.com/locate/ynimg

Dynamic brain network reconfiguration under stress: A multiphase fMRI study

Xiao Luo [a,b], Jiahao Huang [a,b], Kun Shi [a,b], Yiqing Ma [a,b], Yibo Wang [a,b], Xinli Tang [a,b], Xiaolin Zhao [c], Xi Ren [a,b], Juan Yang [a,b,*]

[a] Faculty of Psychology, Southwest University, Chongqing 400715, China
[b] Key Laboratory of Cognition and Personality, Ministry of Education, Southwest University, Chongqing 400715, China
[c] West China Institute of Children's Brain and Cognition, Chongqing University of Education, Chongqing 400715, China

ARTICLE INFO

Keywords:
Stress
Hidden markov modeling (HMM)
Cortisol
Reconfiguration
Allostasis

ABSTRACT

Acute stress induces a dynamic reallocation of neural resources across three distinct phases: Pre-stress, Stress, and Post-stress. Despite extensive research on isolated phases, a critical gap remains in understanding how this resource reconfiguration shapes the brain's dynamic characteristics across the entire temporal continuum. To address this gap, we employed Hidden Markov Modeling (HMM) to investigate whole-brain network dynamics continuously across all phases in two independent cohorts using the ScanSTRESS (n = 77, 35 females) and Montreal Imaging Stress Task (n = 48, 24 females). Our results revealed rapid and reversible spatiotemporal reconfigurations of large-scale brain networks, accompanied by elevated cortisol levels in both cohorts. Specifically, a marked spatiotemporal reconfiguration of brain networks was observed from Pre-stress to Stress phases, characterized by overall suppressed activation of the executive control network, alongside enhanced sensory processing, and increased functional coupling among salience, sensory, and executive networks. These changes reversed during the Post-stress phase, with no significant differences between Pre- and Post-stress phases. Critically, we identified robust individual differences: females exhibited higher state switching rates during stress across both cohorts, and a poorer post-stress recovery index (greater deviation from baseline) was associated with higher depression and anxiety scores. Synthesizing these findings, we propose a Tri-Phase Network Reconfiguration Model positing that allostasis is achieved through phase-specific brain state repertoires and directed transitions. This dynamic framework advances our understanding of stress adaptation and offers testable hypotheses for how these processes may be dysregulated in stress-related psychopathology.

1. Introduction

The brain serves as the central regulator of the stress response, determining threat perception and coordinating adaptive physiological and behavioral reactions (Bhatnagar, 2021; McEwen, 2007). A key mechanism in this process is the dynamic reallocation of neural resources across distinct temporal phases of acute stress: Pre-stress, Stress, and Post-stress (Kühnel et al., 2022; Vaisvaser et al., 2013).

Theoretical models have attempted to describe these dynamics, most notably the Reciprocal Resource Allocation Model, which posits a competitive relationship between the Salience Networks (SN) and Executive Control Networks (ECN), where stress hormones enhance SN activity at the expense of the ECN during stress, followed by a reversion in lengthy post-stress recovery (Hermans et al., 2011, 2014). However, empirical support for this model remains fragmented. Many neuroimaging studies, by focusing solely on either the Stress phase (Goldfarb et al., 2020; Holz et al., 2020; Reynaud et al., 2013; Tobia et al., 2017) or the Post-stress phase using time-averaged approaches (Broeders et al., 2021; Chang et al., 2020; Ginty et al., 2019; Kruse et al., 2018; Veer et al., 2011), provide only static snapshots that cannot delineate the continuous neural transitions implied by the model. For instance, while studies comparing Pre- and Post-stress rest have found connectivity changes (Dimitrov et al., 2018; Zhang et al., 2020), their reliance on simple subtraction of time-averaged signals conflates the frequency and intensity of network engagement, failing to capture the dynamics of the proposed SN-ECN seesaw.

The limitations of a purely dual-network framework became apparent with the introduction of the Triple Network Model in a recent

* Corresponding author.
E-mail address: valleyqq@swu.edu.cn (J. Yang).

https://doi.org/10.1016/j.neuroimage.2026.121903
Received 26 November 2025; Received in revised form 18 March 2026; Accepted 30 March 2026
Available online 31 March 2026
1053-8119/© 2026 The Authors. Published by Elsevier Inc. This is an open access article under the CC BY license (http://creativecommons.org/licenses/by/4.0/).

review (Van Oort et al., 2017). This model, focusing on the Stress phase alone, further emphasized the critical role of the DMN in stress coping and suggested that ECN engagement during stress may not be uniformly suppressed but could follow a more complex, non-linear pattern depending on task demands (Van Oort et al., 2017). This theoretical advancement highlights a critical gap: existing models are primarily descriptive and lack a quantitative account of how neural resources are dynamically reallocated between and within these major networks across the entire stress continuum. While some studies have explored dynamics within the Stress phase (Kühnel et al., 2022; Li et al., 2024; Liu et al., 2023), they still fail to trace the full trajectory of network reconfiguration from pre-stress baseline through stress challenge to post-stress recovery, leaving the core predictions of both major models—particularly regarding the temporal dynamics of the ECN and the role of the DMN—incompletely tested.

Therefore, to move beyond descriptive models and towards a quantitative understanding of dynamic resource reallocation, a method that can directly measure and characterize the fleeting, recurring patterns of whole-brain activity is indispensable (Vidaurre et al., 2021). Prior studies have been forced to either analyze each phase in isolation using time-averaged methods or to apply different models to rest and task data (Van Oort et al., 2017). These approaches conflate the frequency and intensity of network engagement and cannot capture the moment-to-moment transitions into and out of the stressed state, which is fundamentally inaccessible through simple phase-by-phase comparisons. Here, we employed Hidden Markov Model (HMM) to quantitatively answer the fundamental question left open by existing theories: How does the brain dynamically redistribute its resources among major networks at the level of momentary, recurring states to facilitate the transition into and out of a stressed state? Our continuous modeling approach using HMM provides an irreplaceable view of the brain's dynamic trajectory (Stevner et al., 2019; Vidaurre et al., 2017), allowing us to directly observe how neural activity flows from a baseline state, through the stressor, and back to recovery.

To this end, the present study combined two stress paradigms, ScanSTRESS and the Montreal Imaging Stress Task (MIST) (Dedovic et al., 2005; Streit et al., 2014), with fMRI to capture whole-brain dynamics consecutively across Pre-stress, Stress, and Post-stress phases in two independent cohorts. By applying HMM, we aimed to decode the sequence of whole-brain network states that define the stress response, thereby providing a direct, time-resolved assay of neural resource reallocation to test and refine extant theoretical models of acute stress. Building upon above theoretical frameworks, we formulated a set of specific, testable hypotheses regarding the dynamic reallocation of neural resources. First, based on the Reciprocal Resource Allocation Model, we hypothesized that the Stress phase, compared to Pre-stress, would be characterized by: (i) a decreased fractional occupancy (FO) of states dominated by the ECN, reflecting resource withdrawal; (ii) an increased FO of states dominated by the SN and sensory networks, reflecting heightened vigilance; and (iii) a strengthened functional coupling between the SN and sensory networks within these stress-dominant states. Furthermore, we expected these changes to reverse in the Post-stress phase. Second, extending the Triple Network Model's focus on within-stress dynamics, we predicted that the Stress phase would exhibit a higher state switching rate (SR), indicating a more flexible and exploratory neural regime. Critically, we anticipated that this increased switching would not be random but directed, as evidenced by altered transition probabilities funneling brain activity toward the stress states. Furthermore, we conducted exploratory analyses to investigate potential individual differences in these dynamic processes.

2. Materials and method

2.1. Participants

A total of 125 young, healthy college students were recruited in two cohorts, with 77 participants in Cohort 1 and 48 participants in Cohort 2. Female participants were tested during their luteal phase to eliminate the influence of menstrual cycles on their salivary cortisol levels and did not use oral contraceptives leading up to the experiment (Kajantie and Phillips, 2006; Sharma et al., 2020). Four participants were excluded due to excessive head movement (mean framewise displacement (FD) > 0.2) (Parkes et al., 2018), yielding 76 participants in Cohort 1 (34 females; mean age: 20.13 ± 1.94, rang: 18–26 years old) and 45 participants in Cohort 2 (24 females; mean age: 19.09 ± 0.95, range: 18–22 years old) for further brain dynamic analysis. We ascertained all participants' eligibility, current health status, and health behaviors using their self-reports. Exclusion criteria were acute or chronic psychiatric or somatic diseases, psychotropic or glucocorticoid medication intake, and alcohol/drug abuse. All participants provided written informed consent and were informed that they could withdraw at any time. All protocols were complied with the standards of the Declaration of Helsinki and was approved by the Ethics Committee of Southwest University (no. H23090).

2.2. Experimental paradigm

For both Cohort, participants were required to arrive at the laboratory in the mid-afternoon to control the cortisol rhythm. After arriving at the laboratory, participants were asked to rest for 30 min before entering the MRI scanner. A TI image was acquired first, followed by Pre-stress phase, Stress phase, and Post-stress phase. During resting state, participants were instructed to open the eyes, relax, and be still. Subjective stress reports and salivary cortisol data were collected repeatedly from the scanner throughout the experiment (Fig. 1A). Details of two acute stress tasks were presented in our previous study (Liu et al., 2023; Ren et al., 2022).

2.3. Image acquisition

Briefly, MRI data were acquired on a 3T Siemens Prisma MRI scanner (Erlangen, Germany) in Cohort 1 and a 3T Siemens Trio MRI scanner (Munich, Germany) in Cohort 2. Functional images were consecutively collected during Pre-stress, Stress, and Post-stress phases, using T2-weighted gradient echo-planar imaging sequence (for Cohort 1: repetition time = 2000 ms, echo time = 30 ms, slice thickness = 2 mm, matrix = 64 × 64, field of view = 200 × 200 mm^2, and voxel size = 2 × 2 × 2 mm^3; for Cohort 2: repetition time = 2000 ms, echo time = 30 ms, slice thickness = 3 mm, matrix = 64 × 64, field of view = 192 × 192 mm^2, and voxel size = 3 × 3 × 3 mm^3). High-resolution T1-weighted three-dimensional (3D) fast-field echo sequences were obtained for anatomical reference (for Cohort 1: slices = 192, repetition time = 2530 ms, echo time = 2.98 ms, flip angle = 7°, slice thickness = 1 mm, field of view = 256 × 256 mm^2, voxel size = 0.5 × 0.5 × 1 mm^3; for Cohort 2: slices = 176, repetition time = 1900 ms, echo time = 2.52 ms, flip angle = 7°, slice thickness = 1 mm, field of view = 256 × 256 mm^2, voxel size = 1 × 1 × 1 mm^3).

2.4. Image data preprocessing

Preprocessing of the fMRI data for both Cohorts was done using DPABI (a toolbox for Data Processing & Analysis for Brain Imaging, http://rfmri.org/dpabi) (Yan et al., 2016). First, the three-dimensional DICOM image data of each subject were converted to the four-dimensional NIFTI format. The first five volumes for Pre-stress, Stress, and Post-stress phases were discarded respectively to stabilize the magnetic resonance signal (the first four volumes in Cohort 2). The remaining images were corrected for slice acquisition timing, realigned for six head motion parameters correction, spatially normalized into the standard Montreal Neurological Institute (MNI) space in 2 × 2 × 2 mm^3 voxel sizes, and smoothed by convolving a 6-mm isotropic three-dimensional Gaussian kernel. The global signal regression and

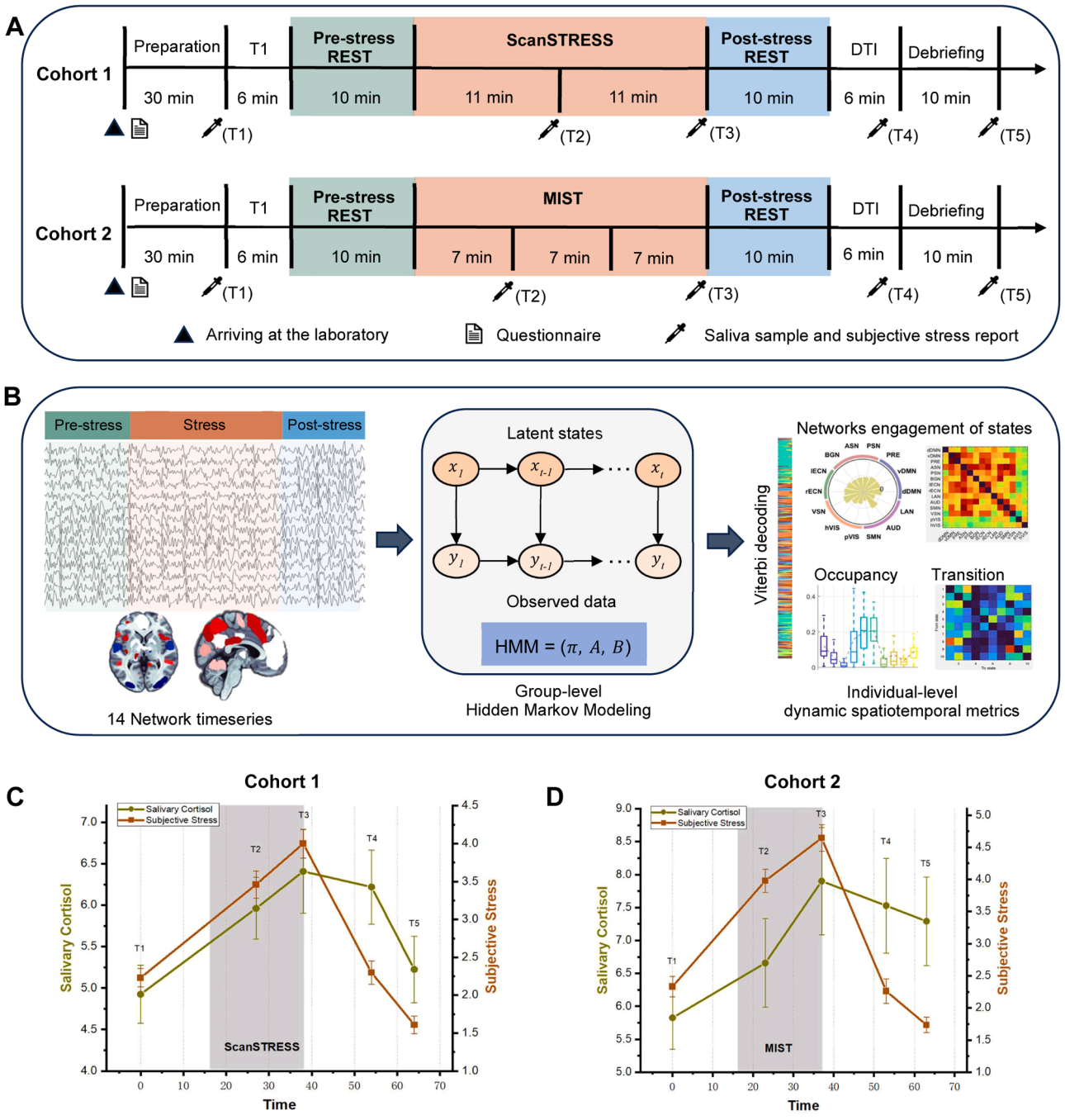


Fig. 1. Experimental design and effective acute stress induction. (A) An overview of the experimental procedure. After arriving at the laboratory, the participants were asked to rest for 30 min before entering the MRI scanner. During the scanning, a T1 image was acquired first, followed by a resting-state image. Immediately, the ScanSTRESS was used to induce a stress response for 22 min in Cohort 1, the MIST was used to induce a stress response for 21 min in Cohort 1. Then, there was another resting-state scan and structural scan; lastly, participants were debriefed for 10 min before they left the laboratory. During this period, participants provided five saliva samples and subjective stress reports. **(B)** BOLD time series during resting-state and task fMRI scanning were extracted as 14 prior-defined brain networks of interest. Hidden Markov model was implemented to estimate network dynamics across Pre-stress, Stress, and Post-stress recovery phase. **(C)** and**Experimental design and effective acute stress induction. (A)** Salivary cortisol and self-reported stress levels during acute stress at all time points in Cohort 1 and Cohort2. The ScanSTRESS and MIST both successfully induced participants' subjective and cortisol stress responses.An overview of the experimental procedure. After arriving at the laboratory, the participants were asked to rest for 30 min before entering the MRI scanner. During the scanning, a T1 image was acquired first, followed by a resting-state image. Immediately, the ScanSTRESS was used to induce a stress response for 22 min in Cohort 1, the MIST was used to induce a stress response for 21 min in Cohort 1. Then, there was another resting-state scan and structural scan; lastly, participants were debriefed for 10 min before they left the laboratory. During this period, participants provided five saliva samples and subjective stress reports. **(B)** BOLD time series during resting-state and task fMRI scanning were extracted as 14 prior-defined brain networks of interest. Hidden Markov model was implemented to estimate network dynamics across Pre-stress, Stress, and Post-stress recovery phase. **(C)** and **(D)** Salivary cortisol and self-reported stress levels during acute stress at all time points in Cohort 1 and Cohort2. The ScanSTRESS and MIST both successfully induced participants' subjective and cortisol stress responses.

motion censoring procedures were not conducted in the present study. The mean FD and scan lengths for each phase in two cohorts were reported in Supplement, Table S1.

2.5. BOLD time series extraction

As shown in Fig. 1B, we employed a predefined 14 networks template (Shirer et al., 2012), covering wide-spread cognitive and affective processing regions that have been widely studied (Meer et al., 2020; Shirer et al., 2012; Zeng et al., 2024). We next extracted preprocessed BOLD time series for each phase continuously by using the 14 network templates, which results in a time series matrix (14 brain networks) × (phase durations). For Cohort 1, time series matrix for Pre-stress phase is 14-by-235, for Stress phase is 14-by-652 and for Post-stress phase is 14-by-235. For Cohort 2, time series matrix for Pre-stress phase is 14-by-238, for Stress phase is 14-by-642 and for Post-stress phase is 14-by-238. For both Cohorts, time series were high-pass filtered at 0.01–0.15 Hz to capture the neural signal associated to both rest and task (Meer et al., 2020) after which the white matter and cerebrospinal fluid, and 24-head movement signals were further used as regressor to remove out from time series. Then, preprocessed time series of 14 networks for the three phases were temporally concatenated together for each participant, yielding a 14-by-1122-time series matrix for Cohort 1 and 14-by-1118-time series matrix for Cohort 2. The concatenated time series were normalized to have zero mean and unit standard deviation across time.

2.6. Hidden Markov model (HMM)

Through Bayesian variations as well as Markovian process, HMM could infer discrete brain states that represent a repertoire of canonical brain networks via Viterbi decoding (Vidaurre et al., 2016). Thus, each state is defined as both mean of each network (activation) and covariance (connectivity) among each network, generated by the Gaussian distribution (Vidaurre et al., 2017). After extracting time series from three stress phases, we concatenated them and conducted HMM using the HMM-MAR MATLAB toolbox (https://github.com/OHBA-analysis/HMM-MAR). Similar to previous studies (Meer et al., 2020; Zeng et al., 2024), free energy as well as Akaike Information Criterion (AIC) was computed at a range from 2 to 16 states with a step of 2 (Supplement, Figure S1). Model priors were set to the toolbox's defaults. We found that 10 states are sufficiently to capture brain sate dynamics across Pre-stress, Stress, and Post-stress. To ensure a stable and robust estimate, we performed 5 independent estimations with different random initializations for the selected $K = 10$ states and retained the model with the lowest free energy. The HMM inversion yields three different types of output: 1) Each state's estimated relative magnitude across 14 brain networks representing relative engagement, together with the functional connectivity/ covariance matrices. 2) State assignment for each time point, each subject, via Viterbi path decoding, based on which we calculated individual-level fractional occupancy (FO) for each state under each specific phase. 3) State switching rate (SR) and transition matrices (one for each participant and phase) were encoding for the transition probability from one state to another. In addition, the robustness of our main findings across a range of state numbers ($K = 8$, 12) is analyzed.

2.7. Comparison of state dynamics between phases

In order to assess brain state dynamics across stress phases, we compared the HMM metrics for each brain state. Specifically, for the FO values that exbibit skewed distribution (Chen et al., 2022), we assessed significant differences between phases (Pre-stress/Stress/Post-stress) by non-parametric test with FDR correction. For the SR values, we conducted repeated ANOVA to detect significant differences between phases, with FDR adjustment (Kuang et al., 2023; Liu et al., 2025). For state transition probability, the Network-Based Statistics toolbox (version 1.2) was used to reveal the network of state transitions that are significantly more expressed during Stress compared to Pre-stress/Post-stress, and during Post-stress compared to Pre-stress phase according to previous studies (Meer et al., 2020; Zeng et al., 2024). Significance determination was computed via nonparametric permutations setting at 5000, alpha setting at 0.05, FWE correction.

2.8. t-SNE embedding visualization for FO

To characterize the evolving distribution patterns across Pre-stress, Stress, and Post-stress phases, we applied t-distributed stochastic neighbor embedding (t-SNE) technique (van der Maaten and Hinton, 2008). This dimensionality reduction technique maps high-dimensional data into a lower-dimensional space while maintaining the local structure between data points. For each participant, brain state distributions under the stress task phase were quantified as 10-element vectors, where each element encoded the relative FO value per phase (Zeng et al., 2024). These vectors, representing all three stress phases, were then subjected to t-SNE analysis. This allowed us to visualize the resulting low-dimensional clusters corresponding to each phase per participant and to depict the relative distances between these phase-specific distributions.

2.9. Neurosynth decoding of states

To reveal the potential neurocognitive processes associated with each state feature, we took advantage of meta-analysis using reverse-inferred similarity-based algorithm by the CANlab toolbox (https://canlab.github.io/). Consistent with previous studies (Yarkoni et al., 2011; Zeng et al., 2024), we correlated each state's activation pattern with the topic term-derived maps from the large-scale Neurosynth platform including nearly 14,300 studies. For each state of interest, we chose the first 4 topics with highest correlations, under which we further chose the first three terms of each topic. This ends up a total of 10 terms for each state ready for Wordcloud visualization. Notably, we manually excluded terms representing irrelevant processes, and merged the similar terms (e.g., action\actions) until the included terms reached 10. Finally, we implemented each state's related terms in a Wordcloud plot and the size of each term is based on its relative correlation value.

2.10. Behavioral measurement

As subjective and endocrine stress reactivities were measured repeatedly throughout the experiment, we calculated the areas under the curve with respect to ground (AUCg), areas under the curve with respect to increases (AUCi), peak response, and reactivity magnitude (peak-baseline) to reflect the level of the cortisol and subject stress response. Besides, the Center for Epidemiologic Studies Depression Scale (CES-D) and the State Anxiety Inventory (SATI) was used to measure depression and anxiety before the stress task.

3. Results

3.1. Cortisol and subjective responses to acute stress

The ScanSTRESS and MIST successfully induced participants' cortisol and subjective responses to acute stress in two cohort. For Cohort 1 (Fig. 1C), repeated ANOVA with time points as a within-subject variable showed that time significantly affected salivary cortisol levels (F (4, 300) = 7.21, $p < 0.001$, $\eta_p^2 = 0.088$), as well as subjective stress levels (F (4, 300) = 82.19, $p < 0.001$, $\eta_p^2 = 0.53$). For Cohort 2 (Fig. 1D), the effect of Time was also significant for the salivary cortisol levels (F (4, 184) = 3.27, $p < 0.05$, $\eta_p^2 = 0.066$), as well as for the subjective stress (F (4, 188) = 95.17, $p < 0.001$, $\eta_p^2 = 0.67$).

3.2. Distinct network expressions of HMM states under acute stress

To detect brain network dynamics across different phases, we implemented HMM for BOLD time series of 14 brain networks during Pre-stress, Stress, and Post-stress phases. Modeling outputs with inferred 10 states featured by distinct network configurations which capture rich brain network dynamics across three phases (Cohort 1: Fig. 2A and Supplement Figure S2; Cohort 2: Supplement Figure S3A).

Brain states are characterized by their distinct fMRI signal loadings onto the 14 brain networks. Take Cohort 1 as an example (Fig. 2B), State 2 (S2) is defined by high fMRI signal in most networks, while S4 and S7 show a relatively uniform fMRI signal across networks. The fMRI signals defining remained brain states load preferentially on one or more specific functional networks. For example, S6 shows a high projection onto salience network, while S9 displays a low projection onto all networks except for the language and sensorimotor networks. The brain states also show idiosyncratic fMRI signal across the 14 brain networks in Cohort 2 (Supplement, Figure S3B). Distinct functional coupling between networks were found in brain states both Cohort (Fig. 2C and Supplement, Figure S3C). We used the Hungarian algorithm to match states across cohorts according to their relative engagement of each network as well as their functional connectivity matrix (Supplement, Figure S4).

3.3. Phase-specific alterations in brain states occupancy

Based on Viterbi-decoded state sequence, we further calculated fractional occupancy (FO; Fig. 3A) of each brain state for Pre-stress, Stress, and Post-stress phases. For Cohort 1, we found significantly higher FO of State 4 (S4), State 5 (S5), and State 6 (S6) during Pre-stress and Post-stress compared to Stress phase. During Stress phase, higher FO of State 2 (S2), State 3 (S3), State 8 (S8), State 9 (S9) compared to the other two phase, and higher FO of State 1 (S1) and State 10 (S10) compared to Prestress alone were observed (all $Ps < 0.05$, FDR corrected). We further calculated state FO for control and stress conditions in Cohort 1, and compared it to supplement the above results (Supplement, Figure S5). The FO of S3, which frequently appeared in the interval between blocks, did not differed in the two blocks. FOs of S1, S2, and S8 in stress blocks were significantly higher than in control blocks, while the difference in S9 failed to pass the multi-comparation correction. Importantly, the FOs of Post-stress phase were not significantly different to Pre-stress phase in any brain states. These results were robust after adjusted for mean FD values of the three phases (Supplement, Figure S6). This unique effect of Stress phase on FO of brain states was also found in Cohort 2 (Supplement, Figure S7A). The matched states of two cohorts are generally in same direction of change from Prestress to Stress and from Stress to Post-stress phases. The FO changes of State 3 and state 10 in Cohort 1 are in the same direction to states 9 of Cohort 2, the second-highest match state.

From a holistic view, we also implemented t-SNE algorithm(van der Maaten and Hinton, 2008) to visualize the distribution of states' FO during three phases, and the low-dimensional clustering result further validates stress-dependent states distributions (Fig. 3B). The distribution of states' FO during Stress phase was distinctly different from Pre-stress and Post-stress phases, but the latter two was similar and coinciding from each other. Notably, we observed similar stress-dependent states distributions across Prestress, Stress, and Post-stress phases in Cohort 2 (Supplement, Figure S7B).

3.4. Phase-specific shifts in brain states transitions

Beyond FO, we examined the difference in state switching rate (SR) during three phases using repeated ANOVA in both cohorts. For Cohort 1, the results showed that phases significantly affected SR (F (2, 150) = 22.47, $p < 0.001$, $\eta_p^2 = 0.23$; Fig. 3C). Post-hoc analysis revealed that the SR increased significantly in the Stress phase compared to the Pre-stress phase, and then decreased significantly in the Post-stress phase ($ps <$ 0.001). However, the frequency of brain states switching during the Pre-stress and Post-stress phase was not significantly different ($p = 0.22$, 95% CI: [−0.025, 0.004]). These results were robust after adjusted for mean FD values of the three phases (F (2, 144) = 9.46, $p < 0.001$, $\eta_p^2 =$ 0.12). Importantly, this effect of phases was exactly repeated in Cohort 2 (F (2, 88) = 16.44, $p < 0.001$, $\eta_p^2 = 0.27$; Supplement, Figure S7C).

To concretely probe the state transition dynamic, we further computed transition probability among brain states across Pre-stress, Stress, and Post-stress phases. Network-based statistics revealed significantly higher transition probabilities to dominant brain states under Stress phase (all $Ps < 0.05$, FDR corrected) (Fig. 3D). Consistent with the results based on FO, no significant difference in edge-by-edge transition between Pre-stress and Post-stress phases were observed (all $Ps > 0.05$, FDR corrected). Importantly, this FO-consistent dominant states as well as unique effects of Stress phase on transition probabilities were also repeated in Cohort 2 (Supplement, Figure S7D).

Based on the combined results of FO and transition probabilities, we identified and validated the dominant states of Stress phase (S2, S3, S8, and S9 in Cohort1; S6, S7, S8, and S9 in Cohort 2), as well as the overlapping dominant states of Pre-stress and Post-stress phases (S4, S5, and S6 in Cohort1; S1, S2, S4, and S5 in Cohort 2) in two Cohorts. Therefore, the Stress phase exhibited unique characteristics in state FO and transition probability, but there were no differences in these metrics between Pre-stress and Post-stress phases. In addition, the robustness of our main findings across a range of state numbers ($K = 8, 12$) is demonstrated in Supplementary Materials (Supplement, Figure S8).

3.5. Individual differences in brain dynamics under stress

We first investigated the sex difference of the brain dynamics during the acute stress process. For both cohorts, females showed a significantly higher overall state switching rate across the entire stress process (Cohort 1: t (74) = 3.392, $p < 0.001$, Cohen's $d = 0.79$ [95% CI: 0.31, 1.26]; Cohort 2: t (43) = 3.379, $p < 0.01$, Cohen's $d = 1.02$ [95% CI: 0.39, 1.64]). MANOVA revealed that this effect was primarily driven by the Stress phase (F (1, 74) = 8.299, $p < 0.01$, $\eta_p^2 = 0.101$ in Cohort 1; F (1, 43) = 8.914, $p < 0.01$, $\eta_p^2 = 0.172$ in Cohort 2), with no significant differences in other phases. As an exploratory analysis (without correction for multiple comparisons across all states and phases), we also examined sex differences in state-specific FO. In Cohort 1, we observed trends ($p < 0.05$ uncorrected) suggesting females spent more time in S6 during Pre-stress and S5 during Post-stress, with less time in S8 and more in S9 during the Stress phase (Fig. 4A). However, these specific state-level patterns were not consistently replicated in Cohort 2 (Supplement, Figure S9A), underscoring the need for caution in their interpretation and highlighting the robustness of the overall SR finding as the primary sex effect.

Then, we explored other individual differences in brain dynamics under stress by linking the state metrics with behavioral measures. Specifically, we calculated the difference of FOs and SR between Stress and Pre-stress phases, and probe their relationships with cortisol and subjective stress responses. In both cohorts, the increase in stress-dominant states in Stress phase compared to the baseline were positively related to subjective stress levels, while the decrease of nonstress states under stress were related to heightened cortisol stress response (Cohort 1: Fig. 4B; Cohort 2: Supplement, Figure S9B). No significant sex interactions were found for changes in SR and state-specific FO. Importantly, we further calculated the total absolute change in FO across 10 states between Post and Pre-stress phases as a recovery index, with higher scores indicating lower recovery capacity. Regression analysis showed that this index was positively related to depression (partial $r = 0.28$, $p < 0.05$) and state anxiety (partial $r = 0.23$, $p < 0.05$) after controlling for sex and mean FD in these two phases (Fig. 4C). However, this relationship was not found in Cohort 2 with a smaller sample.

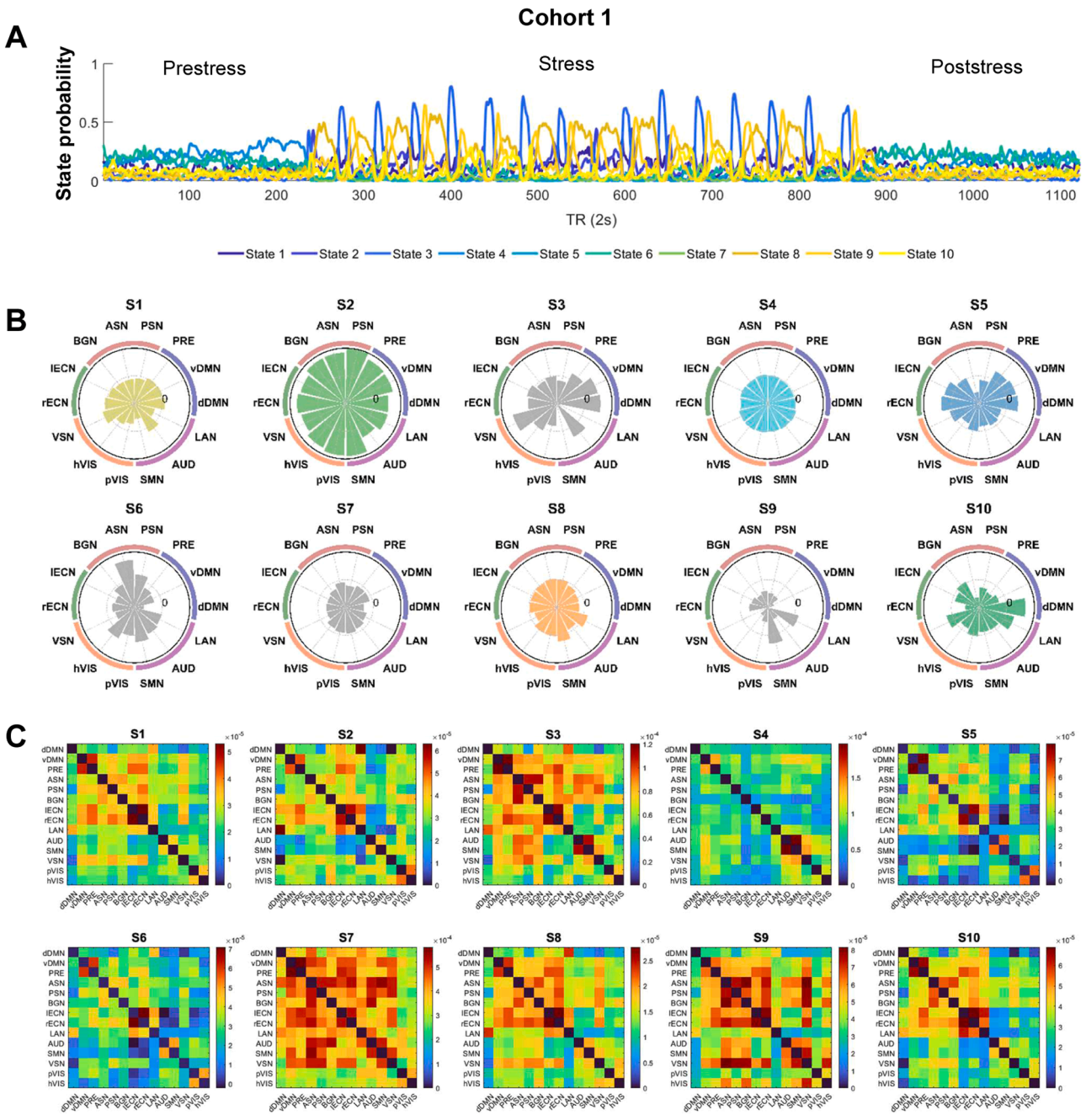


Fig. 2. Brain network configuration patterns of each state across Pre-Stress, Stress, and Post-stress phases in Cohort 1. (A) Hidden Markov Model (HMM) to calculate the probability of latent states being active at each timepoint of the observed time-series. Depicted is the probability of occurrence of any state and each time-point of a part of time-series in Cohort 1. The states do not occur sequentially and any of them might occur at any time-point. **(B)** Polar graphs represent each inferred brain state featured by their relative load of 14 canonical networks in Cohort 1. The value of each bar indicates the relative activity magnitude compared with the average activity inferred from HMM. The order of brain networks in the polar graphs is organized by their functional specialization. **Brain network configuration patterns of each state across Pre-Stress, Stress, and Post-stress phases in Cohort 1. (A)** The functional coupling magnitude between brain networks in each state in Cohort 1. Since the time series for each network within each subject were standardized to ensure that the HMM inference was driven by temporal dynamics rather than differences in signal amplitude, these matrixes cannot be compared across states. Notes: Precuneus Network (PRE), Dorsal and Ventral Default Mode Networks (dDMN and vDMN), Language Network (LAN), Auditory Network (AUD), Sensorimotor Network (SMN), Primary and High Visual Networks (pVIS, hVIS), Visuospatial Network (VSN), Left, and Right Executive Control Networks (lECN, rECN), Basal Ganglia Network (BGN), Anterior, and Posterior Salience Networks (ASN, PSN).Hidden Markov Model (HMM) to calculate the probability of latent states being active at each timepoint of the observed time-series. Depicted is the probability of occurrence of any state and each time-point of a part of time-series in Cohort 1. The states do not occur sequentially and any of them might occur at any time-point. **(B)** Polar graphs represent each inferred brain state featured by their relative load of 14 canonical networks in Cohort 1. The value of each bar indicates the relative activity magnitude compared with the average activity inferred from HMM. The order of brain networks in the polar graphs is organized by their functional specialization. **(C)** The functional coupling magnitude between brain networks in each state in Cohort 1. Since the time series for each network within each subject were standardized to ensure that the HMM inference was driven by temporal dynamics rather than differences in signal amplitude, these matrixes cannot be compared across states. Notes: Precuneus Network (PRE), Dorsal and Ventral Default Mode Networks (dDMN and vDMN), Language Network (LAN), Auditory Network (AUD), Sensorimotor Network (SMN), Primary and High Visual Networks (pVIS, hVIS), Visuospatial Network (VSN), Left, and Right Executive Control Networks (lECN, rECN), Basal Ganglia Network (BGN), Anterior, and Posterior Salience Networks (ASN, PSN).

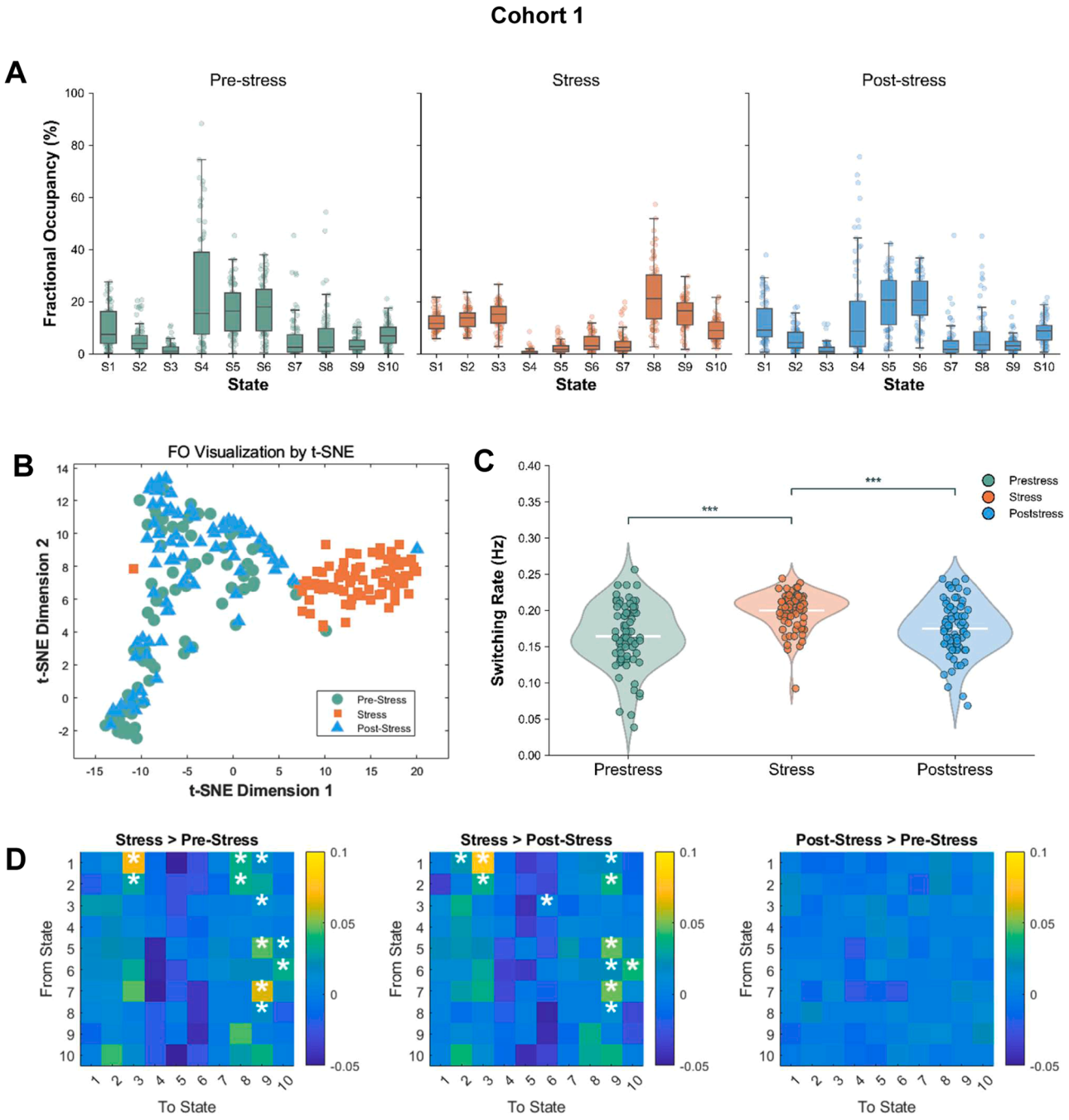


Fig. 3. Brain states dynamics in Cohort 1 showing significant differences between Stress and Pre-stress/Post-stress phases, but not between Pre-stress and Post-stress phase. (A) FO of brain states during Pre-stress, Stress, and Post-stress phases in Cohort 1, respectively. **(B)** t-SNE embedding for distributions visualization of FO from all states for Pre-stress, Stress, and Post-stress phases in Cohort 1. **(C)** SR of brain states during Pre-stress, Stress, and Post-stress phases in Cohort 1, respectively. The solid white lines represent the average value and the downward brackets represent significant differences (FDR corrected). **(D)** Group-averaged transition probability difference between Stress vs. Pre-stress (left), Stress vs. Post-stress (middle), and Post-stress vs. Pre-stress (right) in Cohort 1. Asterisks represent significant higher transitions of Stress compared with Pre-stress and Post-stress phase ($p_{FWE} < 0.05$).

4. Discussion

Dysregulated neurobiological stress responses may increase the occurrence and development of stress-related disorders (Luo et al., 2025; Zhang et al., 2022). Underpinning and explaining the dynamic neural mechanisms underlying acute stress holds significant importance (Kühnel et al., 2022). Combining the ScanSTRESS and MIST with functional MRI, this study employed HMM to delineate the spatiotemporal dynamics of large-scale brain networks across the complete, continuous trajectory of acute stress in two independent cohorts. Our findings provide compelling evidence for rapid and reversible reconfigurations of brain network states that support active adaptation to stress and achieve allostasis (McEwen, 1998). Below, we discuss the dynamic characteristics of each phase, integrate these findings into a novel theoretical model, and consider important sex differences in stress-induced brain dynamics.

4.1. Dynamics characteristics of the stress phase

The Stress phase demonstrated a fundamentally distinct dynamic

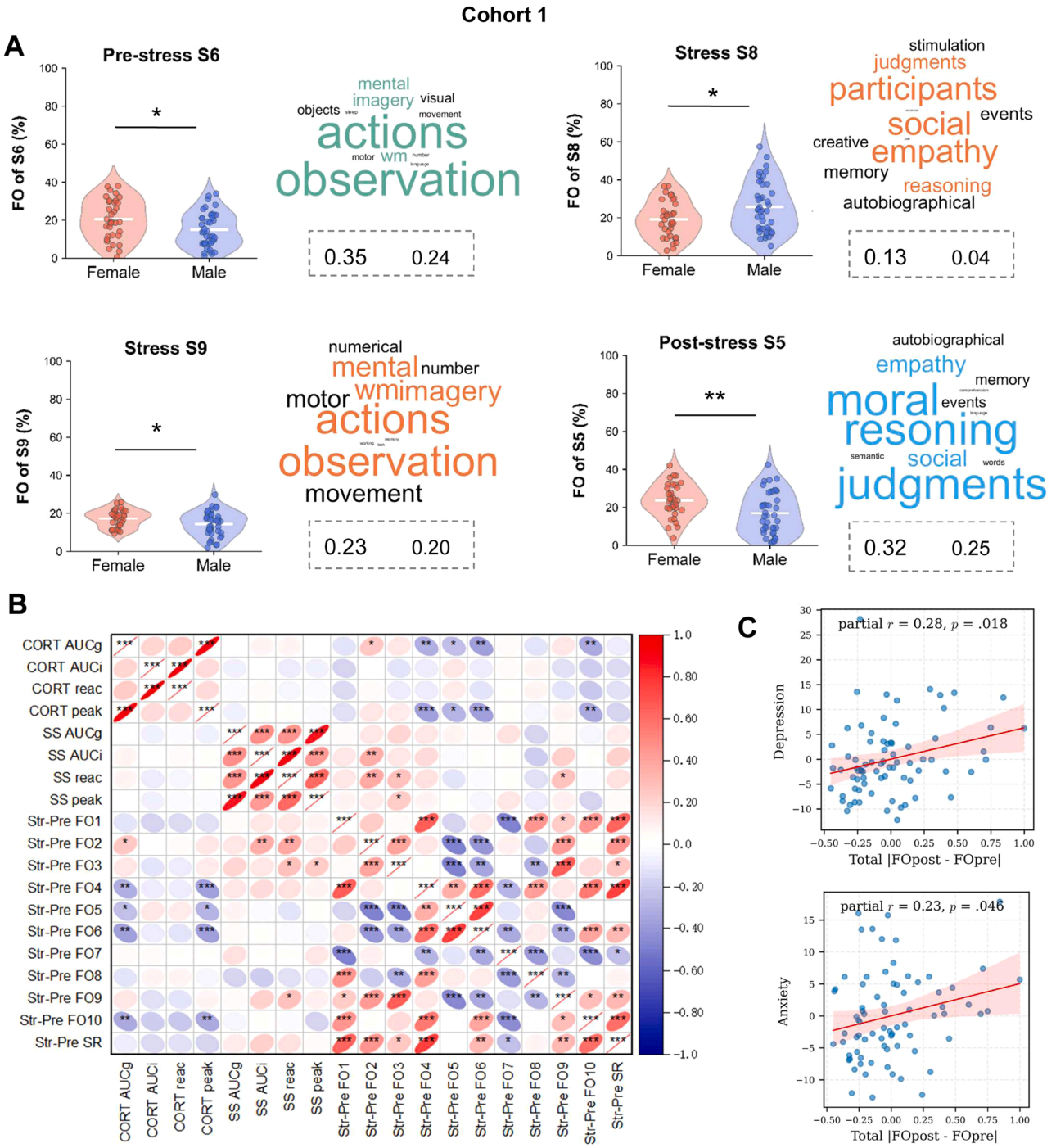


Fig. 4. Individual differences in brain dynamics during stress in Cohort 1. (A) Phase-specific sex differences in brain states occupancy in Cohort 1. Females displayed higher FO value of S6 during Pre-stress phase only, showed lower FO value of S8 but higher FO of S9 during Stress phase, and displayed higher FO value of S5 during Post-stress phase only. Wordcloud plots for Neurosynth-based decoding terms for states of interest. The font size of each term in each plot is based on its relative decoded correlation value, and we list the top and last correlation values below the plot with their font size relative to the correlation values. **(B)** The difference of FOs and SR between Stress and Pre-stress phases related to cortisol and subjective stress response in Cohort 1. **(C)** The total absolute change in FO across 10 states between Post and Pre-stress phases was positively related to depression (partial $r = 0.28$, $p < 0.05$) and state anxiety (partial $r = 0.28$, $p < 0.05$) after controlling for sex and mean FD. The solid line represents the least-squares fit, and the shading represents the 95% CI of the linear fit. * $p < 0.05$, ** $p < 0.01$, *** *Individual differences in brain dynamics during stress in Cohort 1. (A)* < 0.001, non-corrected. Phase-specific sex differences in brain states occupancy in Cohort 1. Females displayed higher FO value of S6 during Pre-stress phase only, showed lower FO value of S8 but higher FO of S9 during Stress phase, and displayed higher FO value of S5 during Post-stress phase only. Wordcloud plots for Neurosynth-based decoding terms for states of interest. The font size of each term in each plot is based on its relative decoded correlation value, and we list the top and last correlation values below the plot with their font size relative to the correlation values. **(B)** The difference of FOs and SR between Stress and Pre-stress phases related to cortisol and subjective stress response in Cohort 1. **(C)** The total absolute change in FO across 10 states between Post and Pre-stress phases was positively related to depression (partial $r = 0.28$, $p < 0.05$) and state anxiety (partial $r = 0.28$, $p < 0.05$) after controlling for sex and mean FD. The solid line represents the least-squares fit, and the shading represents the 95% CI of the linear fit. * $p < 0.05$, ** $p < 0.01$, *** $p < 0.001$, non-corrected.

profile. The overall suppressed ECN activation alongside enhanced sensory processing and increased functional coupling among the SN, sensory, and executive networks aligns with and dynamically refines existing models (Hermans et al., 2014; Van Oort et al., 2017). The general dampening of the ECN is consistent with the Reciprocal Resource Allocation Model's postulate of a stress-induced shift of resources away from this network (Hermans et al., 2014), transiently impairing prefrontal cortex-mediated top-down executive functions (Arnsten, 2009; Zhang et al., 2019). Concurrently, the heightened sensory activation and its strengthened coupling with the SN reflect an adaptive reallocation of resources towards rapid threat detection and environmental monitoring (Kim and Kim, 2023; Luo et al., 2025), priming the organism for a swift response, as suggested by the Triple Network Model (Van Oort et al., 2017).

Crucially, our dynamic approach reveals a more complex narrative than a simple network suppression or enhancement. The finding that the ECN and DMN were actively recruited in specific states during the stress phase suggests a state-dependent, strategic engagement of these networks. The ECNs continued to function in specific states to counter threats and fulfill cognitive tasks (see S2 in Cohort 1, S9 in Cohort 2), while the DMNs also playing a role in emotion appraisal and self-referential processing (see S3 in Cohort 1, S9 in Cohort 2) (Li et al., 2024; Zhang et al., 2019). Functional coupling of ventral DMN with other networks were observed in Stress phase, which was even more pronounced in Cohort 2, suggesting consistent emotion processing and self-evaluation during the Stress phase. This indicates that allostasis is achieved not through monolithic network changes, but through a refined, momentary recruitment of networks for specific appraisal (DMN) or regulatory (ECN) functions within the broader stress response (Chattarji et al., 2015).

Our HMM analysis also revealed that the brain operates with greater global flexibility during Stress phase. The significant increase in the state switching rate (SR) during the Stress phase in both cohorts indicates a less stable, more explorative neural regime—the brain explores its state space more rapidly to meet changing environmental demands (Vidaurre et al., 2021). Critically, the brain does not transition randomly during stress, instead, transition into specific, dominant stress states. This suggests that the stress response involves a coordinated, non-random search through the state space, effectively funneling brain activity toward configurations that are adaptive under threat (Bhatnagar, 2021; Hermans et al., 2014). This heightened dynamism is a key dynamic characteristic that static methods cannot capture and may be fundamental to the brain's ability to rapidly sample different functional configurations to identify an optimal state for dealing with the challenging situation (Vidaurre et al., 2017).

It is worth noting that a critical consideration in any stress fMRI study is the inherent confound between the emotional stress response and general cognitive task engagement (Noack et al., 2019; Van Oort et al., 2017). Although our stress paradigms involve cognitive tasks by design, several lines of evidence from our study suggest that the observed stress states are not simply cognitive states. First, our within-stress phase analysis (Supplement, Figure S5) directly compared HMM state occupancy during stress blocks versus interleaved control blocks. States identified as stress-dominant showed significantly higher FO during stress blocks specifically, demonstrating that their expression is not uniform across all task periods. Second, the increase in FO of stress-dominant states was positively correlated with individual subjective stress levels (Fig. 4B), providing a direct link between the brain state and the psychological experience of stress. Third, the reversal of all dynamic metrics (FO, SR, transitions) to pre-stress levels during the post-stress resting phase, despite the absence of any cognitive task, further confirms that these dynamics were specifically tied to the stress manipulation and its aftermath, not to sustained cognitive effort. Taken together, these control analyses and brain-behavior correlations provide strong evidence that the identified dynamic reconfigurations are indeed stress-specific, reflecting the neural correlates of allostasis rather than merely task engagement.

4.2. Dynamic characteristics of the pre-stress and post-stress phases

Another salient finding of our study is the remarkable similarity in brain network dynamics between the Pre-stress and Post-stress phases, despite the profound perturbation induced by acute stress. In both cohorts, we observed no significant differences in FO of brain states or transition probabilities between these two phases. Thus, we provide robust, replicable evidence that acute stress induces a rapid and largely reversible reconfiguration of whole-brain network dynamics, fulfilling a key prediction of allostasis—the brain's capacity to achieve stability through change (McEwen and Gianaros, 2011).

The dominant states characterizing both Pre-stress and Post-stress phases appear to represent a baseline dynamic regime that supports normal cognitive functioning and internal monitoring. One recurring type of state was defined by relatively uniform, low-amplitude activation across all major networks, suggesting a balanced, globally integrated mode of brain function typical of non-demanding conditions (Raichle et al., 2001). Other prominent states featured either the activation of the ECNs manifested prefrontal cortex-mediated top-down executive functions (Arnsten, 2009; Luo et al., 2025), the activation of the DMNs involved spontaneous and self-generated thought (Andrews-Hanna et al., 2014; Buckner et al., 2008), or the selective engagement of the anterior SN, consistent with a baseline level of interoception (Craig, 2009) and environmental monitoring (Hermans et al., 2014). Crucially, the functional coupling between networks within these states was generally of moderate and balanced intensity, standing in clear contrast to the robust and specific connections that characterized the Stress phase. For instance, even in states where the ECN and DMN were co-activated, they did not exhibit the strong anti-correlation typical of focused task execution, nor the exaggerated positive coupling found under stress (Van Oort et al., 2017). Similarly, the anterior SN operated without the intensified coupling to sensory systems that defined the stress response (Arnsten, 2009).

Previous studies have investigated the resting-state neural changes of specific brain region before and after acute stress (Dimitrov et al., 2018; Zhang et al., 2020), as well as resting-state activity and FC of several brain regions in the Post-stress phase alone (Chang et al., 2020; Ginty et al., 2019; Kruse et al., 2018; Veer et al., 2011). Combining two independent healthy cohorts fulfilling different psychosocial stress tasks, our results consistently suggested that the brain can reverse the neural spatiotemporal reconfigurations to the Pre-stress mode at the network level in the Post-stress phase. The complete reversal of these configurations in the post-stress phase, with no significant differences from pre-stress, underscores the brain's remarkable capacity for dynamic re-equilibration, a hallmark of adaptive stress resilience (Akil and Nestler, 2023; Bhatnagar, 2021). Furthermore, this reverse after an experimentally induced stress was not as time-costing as the Reciprocal Resource Allocation Model has depicted, at least in a network level. We propose that a failure to down-regulate this high-flexibility, directed mode post-stress might be a feature of maladaptive stress responses seen in some psychopathologies (Kalisch et al., 2017).

4.3. Individual differences in stress-induced brain dynamics

First, we found significant sex differences in stress neurodynamics, most robustly evidenced by a higher state switching rate in females during the Stress phase across both cohorts. This suggests that female brains may employ a more labile or explorative dynamic strategy in response to acute stressors (Bhatnagar, 2021; Vidaurre et al., 2017). This may lie in underlying neuroendocrine factors. For instance, estrogen and progesterone are known to modulate the structure and function of stress-sensitive brain regions like the amygdala and prefrontal cortex (Kajantie and Phillips, 2006; Toffoletto et al., 2014), potentially influencing the flexibility of large-scale network dynamics. Our experimental

design, which tested all female participants during the luteal phase to control for menstrual cycle effects (Kajantie and Phillips, 2006), may have inadvertently reduced within-female variance but also limits the generalizability of our findings to other cycle phases. Our exploratory state-level FO findings, while intriguing, were inconsistent across cohorts and should be interpreted cautiously. Specifically, early in the Pre-stress phase, females remained in the state of highly activated SNs especially anterior SN (see S6 in Cohort 1) for a longer period of time, ready to spot threats or important issues and to take actions to address them (Van Oort et al., 2017; Zhang et al., 2022). During the Stress phase, males tend to stay longer in states recruited more ECNs, while females tend to remain in a more sensory-dominant state (S8 vs. S9 in Cohort 1, S7 vs. S8 in Cohort 2). Furthermore, females remained in the state that involved in social judgment and moral reasoning (see S5 in Cohort 1), with highly activated DMNs and ECNs, suggesting that females were more likely to immerse in self-referential and emotional processing during the Post-stress phase (Van Oort et al., 2017; Zhang et al., 2019).

Beyond sex, our exploration of individual differences revealed meaningful links between brain dynamics and stress response, depression and anxiety scores, providing initial evidence for the clinical relevance of our dynamic markers. First, we found that the magnitude of change in brain dynamics from Pre-stress to Stress was behaviorally relevant. The increase in FO of stress-dominant states was positively related to subjective stress levels, while the concomitant decrease in non-stress states was associated with a heightened cortisol response. This dissociation suggests that different aspects of the neural reconfiguration may track distinct facets of the stress experience: the engagement of a stress-specific neural coalition reflects the conscious perception of stress, whereas the disengagement of a baseline neural regime is more closely tied to the underlying neuroendocrine cascade (Goldfarb et al., 2020; Kühnel et al., 2022). Second, we observed that individuals who showed a greater overall deviation from their baseline neural configuration after stress reported higher levels of depression and state anxiety. This finding is pivotal as it moves beyond characterizing a normative response and begins to identify a potential neural biomarker of vulnerability. A larger post-stress deviation suggests a slower or incomplete return to a pre-stress neural equilibrium, which could represent a state of prolonged allostatic load (McEwen and Gianaros, 2011). This might be a subtle indicator of reduced resilience, making an individual more susceptible to the cumulative wear-and-tear of daily stressors (McEwen, 2007; McEwen and Gianaros, 2011). These findings, while preliminary, directly respond to calls for identifying

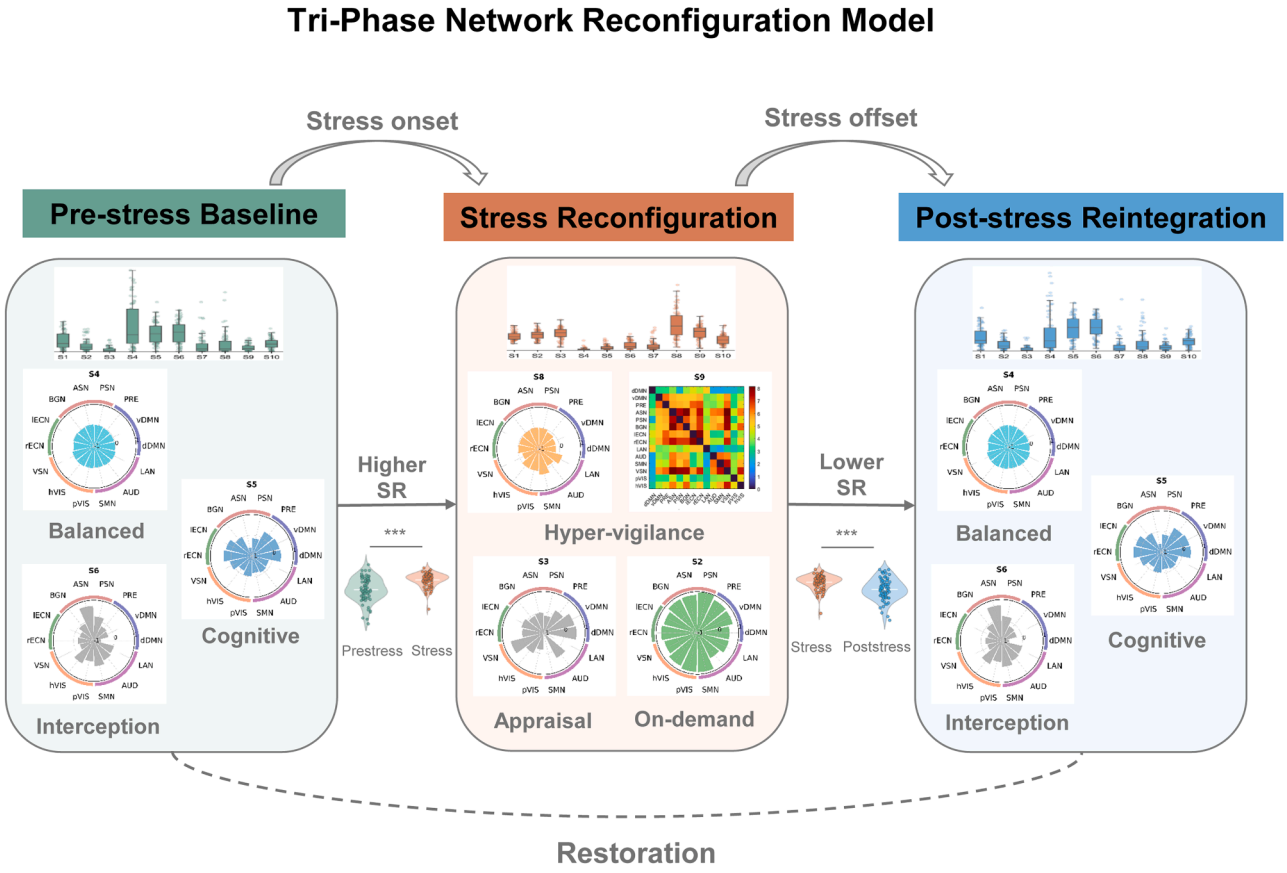


Fig. 5. The proposed Tri-Phase Network Reconfiguration Model of acute stress. This model conceptualizes the brain's stress response as a cycle of network reorganization across three dynamic phases. (1) Pre-stress Baseline Phase: Characterized by a stable set of dominant brain states with moderate switching rates, representing the brain's functional architecture during non-stress conditions. (2) Stress Reconfiguration Phase: Marked by the dissolution of baseline network configurations and the emergence of a transient stress coping coalition. This phase is defined by engagement of stress-specific brain states, significantly increased state switching rates, and strengthened coupling within the salience-sensory hyper-vigilance alliance while maintaining targeted salience-executive connectivity for on-demand cognitive control. (3) Post-stress Reintegration Phase: Characterized by the dissolution of the stress coalition and return to the baseline dynamic regime, with restoration of Pre-stress-like state distributions and switching rates. This model conceptualizes the brain's stress response as a cycle of network reorganization across three dynamic phases. (1) Pre-stress Baseline Phase: Characterized by a stable set of dominant brain states with moderate switching rates, representing the brain's functional architecture during non-stress conditions. (2) Stress Reconfiguration Phase: Marked by the dissolution of baseline network configurations and the emergence of a transient stress coping coalition. This phase is defined by engagement of stress-specific brain states, significantly increased state switching rates, and strengthened coupling within the salience-sensory hyper-vigilance alliance while maintaining targeted salience-executive connectivity for on-demand cognitive control. (3) Post-stress Reintegration Phase: Characterized by the dissolution of the stress coalition and return to the baseline dynamic regime, with restoration of Pre-stress-like state distributions and switching rates.

neurodynamic markers of stress vulnerability and offer a specific, quantifiable target for future studies on stress, resilience, and intervention efficacy.

4.4. A tri-phase network reconfiguration model

Based on these distinct phase characteristics, we propose a Tri-Phase Network Reconfiguration Model of acute stress that extends existing theoretical frameworks (Fig. 5). This model conceptualizes the brain's stress response as a cycle of network reorganization across three dynamic phases:

Pre-stress Baseline Phase: Characterized by a stable set of dominant brain states with moderate switching rates, representing the brain's functional architecture during non-stress conditions.

Stress Reconfiguration Phase: Marked by the dissolution of baseline network configurations and the emergence of a transient stress coping coalition. This phase is defined by engagement of stress-specific brain states, significantly increased state switching rates, and strengthened coupling within the salience-sensory hyper-vigilance alliance while maintaining targeted salience-executive connectivity for on-demand cognitive control.

Post-stress Reintegration Phase: Characterized by the dissolution of the stress coalition and return to the baseline dynamic regime, with restoration of Pre-stress-like state distributions and switching rates.

This model advances beyond existing frameworks by emphasizing the dynamic transitions between discrete brain states rather than average activation levels. It accounts for both the overall suppression of executive networks during stress and their intermittent recruitment in specific states, resolving apparent contradictions in the literature regarding executive function during stress. Furthermore, the model provides a dynamic interpretation of allostasis as the brain's capacity to transition between these phase-specific dynamic regimes.

4.5. Implications for chronic stress and psychopathology

While our study focused on healthy individuals undergoing acute stress, the dynamic markers we identified offer a normative baseline against which maladaptive patterns could be compared. Below, we outline several hypotheses that emerge from our Tri-Phase Network Reconfiguration Model, which await direct testing in future studies.

Chronic Stress. Chronic stress exposure may impair the brain's dynamic range, potentially leading to a less flexible system(Bhatnagar, 2021). Based on our framework, one might expect to observe: (i) a blunted increase in SR during exposure to a novel acute stressor, indicating reduced adaptive flexibility; and (ii) an incomplete reintegration in the Post-stress phase, characterized by residual occupancy of stress-dominant states and a failure to fully return to baseline FO and transition probabilities. Such patterns would be consistent with the concept of allostatic load, where cumulative wear and tear reduces the system's capacity for dynamic adaptation (McEwen and Gianaros, 2011).

Stress-Related Psychopathology. Extending this logic, different stress-related disorders may exhibit distinct signatures of dynamic dysfunction, though this remains a speculative but testable possibility. In Post-Traumatic Stress Disorder (PTSD), where threat reactivity persists even after stressor cessation (Shalev et al., 2017), one might hypothesize a failure to down-regulate the stress coalition post-threat. This could manifest as persistently high occupancy of stress-dominant states and an elevated SR during the Post-stress phase, potentially reflecting a state of perpetual readiness (Shalev et al., 2017). In anxiety disorders, characterized by hypervigilance and exaggerated threat detection (Grupe and Nitschke, 2013), the Stress phase itself might be marked by an excessively high but less directed SR, a hyper-exploratory yet inefficient neural response, possibly coupled with heightened transitions into sensory-dominant states. In major depressive disorder, often associated with reduced cognitive flexibility and blunted stress engagement (Stange et al., 2017), one might expect a rigidity pattern: an inability to sufficiently disengage from a baseline mode, resulting in a blunted increase in SR during stress and insufficient recruitment of ECN-dominant states (Javaheripour et al., 2023).

Notably, our preliminary finding that a poorer recovery index (greater total change in FO from pre- to post-stress) was associated with higher depression and anxiety scores in Cohort 1 lends initial, albeit tentative, support to this framework. This observation raises the possibility that even individuals with subclinical symptoms may exhibit subtle after-effects of stress, struggling to fully reintegrate their neural dynamics back to baseline. However, given the exploratory nature of this finding and its lack of replication in Cohort 2, it should be interpreted with caution and requires confirmation in larger, more diverse samples, particularly those including clinical populations.

4.6. Limitations

Several limitations should be acknowledged. First, while HMM excels at identifying discrete, recurring states, the continuous nature of brain activity might also be captured by other analytical frameworks. Second, the psychological interpretation of the HMM states, though aided by neurosynth decoding, requires further validation through tasks designed to probe specific cognitive functions concurrently with fMRI. Third, the duration of the Pre-stress and Post-stress phases were not as long as the Stress phase, previous studies may extend the resting-state scan to verify our findings. Finally, our sample, while including two cohorts, consisted of healthy young adults, may limit the exploration of individual differences in stress resilience or vulnerability. Generalizability to clinical populations or different age groups remains to be established. Investigating how pre-existing traits modulate these dynamic trajectories could yield valuable insights for personalized interventions.

5. Conclusion

In summary, this multiphase fMRI study elucidates the dynamic brain network reconfigurations that underpin the acute stress response and subsequent recovery. The proposed Tri-Phase Network Reconfiguration Model integrates these findings into a coherent framework that emphasizes the dynamic nature of stress adaptation. The reversible reconfiguration from baseline to stress-specific dynamics and back again provides a neural signature of stress adaptation in healthy individuals, while the identified sex differences highlight important individual variations in these dynamic strategies. These insights advance provides our understanding of the neurodynamic mechanisms of allostasis and open new avenues for identifying biomarkers of stress vulnerability and resilience.

Funding

This work was supported by the Natural Science Foundation of Chongqing [CSTB2023NSCQ-MSX0139], and National Natural Science Foundation of China [32271133], and the National Key Research and Development Program of China [2022ZD0211000].

Data and code availability statement

The data and code that supports the findings of this study will be available from the corresponding author upon request.

CRediT authorship contribution statement

Xiao Luo: Writing – review & editing, Writing – original draft, Visualization, Software, Methodology, Formal analysis, Data curation, Conceptualization. **Jiahao Huang:** Writing – review & editing, Visualization. **Kun Shi:** Writing – review & editing. **Yiqing Ma:** Writing –

review & editing. **Yibo Wang:** Writing – review & editing, Methodology. **Xinli Tang:** Writing – review & editing, Methodology. **Xiaolin Zhao:** Investigation. **Xi Ren:** Investigation. **Juan Yang:** Writing – review & editing, Supervision, Project administration, Funding acquisition.

Declaration of competing interest

The authors have declared no conflict of interest.

Acknowledgments

We are grateful to *PSCN lab* members for data collection and all participants for their contribution to this study.

Supplementary materials

Supplementary material associated with this article can be found, in the online version, at doi:10.1016/j.neuroimage.2026.121903.

References

Akil, H., Nestler, E.J., 2023. The neurobiology of stress: vulnerability, resilience, and major depression. Proceed. Nat. Acad. Sci. 120 (49), e2312662120. https://doi.org/10.1073/pnas.2312662120.

Andrews-Hanna, J.R., Smallwood, J., Spreng, R.N., 2014. The default network and self-generated thought: component processes, dynamic control, and clinical relevance. Ann. N. Y. Acad. Sci. 1316 (1), 29–52. https://doi.org/10.1111/nyas.12360.

Arnsten, A.F.T., 2009. Stress signalling pathways that impair prefrontal cortex structure and function. Nat. Rev. Neurosci. 10 (6), 410–422. https://doi.org/10.1038/nrn2648.

Bhatnagar, S., 2021. Rethinking stress resilience. Trends. Neurosci. 44 (12), 936–945. https://doi.org/10.1016/j.tins.2021.09.005.

Broeders, T.A.A., Schoonheim, M.M., Vink, M., Douw, L., Geurts, J.J.G., Van Leeuwen, J. M.C., Vinkers, C.H., 2021. Dorsal attention network centrality increases during recovery from acute stress exposure. NeuroImage: Clinic. 31, 102721. https://doi.org/10.1016/j.nicl.2021.102721.

Buckner, R.L., Andrews-Hanna, J.R., Schacter, D.L., 2008. *The brain's default network: anatomy, function, and relevance to disease*. Ann. N. Y. Acad. Sci. 1124 (1), 1–38. https://doi.org/10.1196/annals.1440.011.

Chang, J., Hu, J., Li, C.S.R., Yu, R., 2020. Neural correlates of enhanced response inhibition in the aftermath of stress. Neuroimage 204, 116212. https://doi.org/10.1016/j.neuroimage.2019.116212.

Chattarji, S., Tomar, A., Suvrathan, A., Ghosh, S., Rahman, M.M., 2015. Neighborhood matters: divergent patterns of stress-induced plasticity across the brain. Nat. Neurosci. 18 (10), 1364–1375. https://doi.org/10.1038/nn.4115.

Chen, K., Li, C., Sun, W., Tao, Y., Wang, R., Hou, W., Liu, D.-Q., 2022. Hidden Markov modeling reveals prolonged "baseline" State and shortened antagonistic State across the adult lifespan. Cerebral Cortex 32 (2), 439–453. https://doi.org/10.1093/cercor/bhab220.

Craig, A.D., 2009. How do you feel — now? the anterior insula and human awareness. Nat. Rev. Neurosci. 10 (1), 59–70. https://doi.org/10.1038/nrn2555.

Dedovic, K., Renwick, R., Mahani, N., Engert, V., Lupien, S., Pruessner, J., 2005. The montreal imaging stress task: using functional imaging to investigate the effects of perceiving and processing psychosocial stress in the human brain. J. Psychiatry Neurosci. 30 (5), 319–325. WOS:000231412400003.

Dimitrov, A., Demin, K., Fehlner, P., Walter, H., Erk, S., Veer, I.M., 2018. Differences in neural recovery from acute stress between cortisol responders and non-responders. Front. Psychiatry 9, 631. https://doi.org/10.3389/fpsyt.2018.00631.

Ginty, A.T., Kraynak, T.E., Kuan, D.C., Gianaros, P.J., 2019. Ventromedial prefrontal cortex connectivity during and after psychological stress in women. Psychophysiology. 56 (11), e13445. https://doi.org/10.1111/psyp.13445.

Goldfarb, E.V., Rosenberg, M.D., Seo, D., Constable, R.T., Sinha, R., 2020. Hippocampal seed connectome-based modeling predicts the feeling of stress. Nat. Commun. 11 (1), 2650. https://doi.org/10.1038/s41467-020-16492-2.

Grupe, D.W., Nitschke, J.B., 2013. Uncertainty and anticipation in anxiety: an integrated neurobiological and psychological perspective. Nat. Rev. Neurosci. 14 (7), 488–501. https://doi.org/10.1038/nrn3524.

Hermans, E.J., Henckens, M.J.A.G., Joëls, M., Fernández, G., 2014. Dynamic adaptation of large-scale brain networks in response to acute stressors. Trends. Neurosci. 37 (6), 304–314. https://doi.org/10.1016/j.tins.2014.03.006.

Hermans, E.J., Van Marle, H.J.F., Ossewaarde, L., Henckens, M.J.A.G., Qin, S., Van Kesteren, M.T.R., Schoots, V.C., Cousijn, H., Rijpkema, M., Oostenveld, R., Fernández, G., 2011. Stress-related noradrenergic activity prompts large-scale neural network reconfiguration. Science (1979) 334 (6059), 1151–1153. https://doi.org/10.1126/science.1209603.

Holz, N.E., Tost, H., Meyer-Lindenberg, A., 2020. Resilience and the brain: a key role for regulatory circuits linked to social stress and support. Mol. Psychiatry 25 (2), 379–396. https://doi.org/10.1038/s41380-019-0551-9.

Javaheripour, N., Colic, L., Opel, N., Li, M., Maleki Balajoo, S., Chand, T., Van Der Meer, J., Krylova, M., Izyurov, I., Meller, T., Goltermann, J., Winter, N.R., Meinert, S., Grotegerd, D., Jansen, A., Alexander, N., Usemann, P., Thomas-Odenthal, F., Evermann, U., Walter, M., 2023. Altered brain dynamic in major depressive disorder: state and trait features. Transl. Psychiatry 13 (1), 261. https://doi.org/10.1038/s41398-023-02540-0.

Kajantie, E., Phillips, D.I.W., 2006. The effects of sex and hormonal status on the physiological response to acute psychosocial stress. Psychoneuroendocrinology. 31 (2), 151–178. https://doi.org/10.1016/j.psyneuen.2005.07.002.

Kalisch, R., Baker, D.G., Basten, U., Boks, M.P., Bonanno, G.A., Brummelman, E., Chmitorz, A., Fernàndez, G., Fiebach, C.J., Galatzer-Levy, I., Geuze, E., Groppa, S., Helmreich, I., Hendler, T., Hermans, E.J., Jovanovic, T., Kubiak, T., Lieb, K., Lutz, B., Kleim, B., 2017. The resilience framework as a strategy to combat stress-related disorders. Nat. Hum. Behav. 1 (11), 784–790. https://doi.org/10.1038/s41562-017-0200-8.

Kim, E.J., Kim, J.J., 2023. Neurocognitive effects of stress: a metaparadigm perspective. Mol. Psychiatry 28 (7), 2750–2763. https://doi.org/10.1038/s41380-023-01986-4.

Kruse, O., Tapia León, I., Stalder, T., Stark, R., Klucken, T., 2018. Altered reward learning and hippocampal connectivity following psychosocial stress. Neuroimage 171, 15–25. https://doi.org/10.1016/j.neuroimage.2017.12.076.

Kuang, N., Liu, Z., Yu, G., Wu, X., Becker, B., Fan, H., Peng, S., Zhang, K., Zhao, J., Kang, J., Dong, G., Zhao, X., Sahakian, B.J., Robbins, T.W., Cheng, W., Feng, J., Schumann, G., Palaniyappan, L., Zhang, J., 2023. Neurodevelopmental risk and adaptation as a model for comorbidity among internalizing and externalizing disorders: genomics and cell-specific expression enriched morphometric study. BMC. Med. 21 (1), 291. https://doi.org/10.1186/s12916-023-02920-9.

Kühnel, A., Czisch, M., Sämann, P.G., Binder, E.B., Kroemer, N.B., Brückl, T., Spoormaker, V.I., Erhardt, A., Grandi, N.C., Ziebula, J., Elbau, I.G., Namendorf, T., Lucae, S., 2022. Spatiotemporal dynamics of stress-induced network reconfigurations reflect negative affectivity. Biol. Psychiatry 92 (2), 158–169. https://doi.org/10.1016/j.biopsych.2022.01.008.

Li, Y., Liu, Y., Zhao, X., Ren, Y., Hu, W., Yang, Z., Yang, J., 2024. Static and temporal dynamic in functional connectivity of large-scale brain networks during acute stress regulate stress resilience differently: the promotion role of trait resilience. Neuroscience 551, 132–142. https://doi.org/10.1016/j.neuroscience.2024.05.021.

Liu, Y., Peng, S., Wu, X., Liu, Z., Lian, Z., Fan, H., Kuang, N., Gu, X., Yang, S., Hu, Y., Jiang, X., Zhang, Y., Cheng, W., Feng, J., Sahakian, B.J., Zhao, X., Robbins, T.W., Becker, B., Zhang, J., 2025. Neural, cognitive and psychopathological signatures of a prosocial or delinquent peer environment during early adolescence. Dev. Cogn. Neurosci. 73, 101566. https://doi.org/10.1016/j.dcn.2025.101566.

Liu, Y., Zhao, X., Hu, W., Ren, Y., Wei, Z., Ren, X., Tang, Z., Wang, N., Chen, H., Li, Y., Shi, Z., Qin, S., Yang, J., 2023. Neural habituation during acute stress signals a blunted endocrine response and poor resilience. Psychol. Med. 1–11. https://doi.org/10.1017/S0033291723001666.

Luo, X., Zhao, X., Wang, S., Shi, K., Huang, J., Yang, J., 2025. Limbic functional connectivity during stress induction and post-stress rest regulates cortisol stress reactivity and recovery differently. Biol. Psychol., 109110 https://doi.org/10.1016/j.biopsycho.2025.109110.

McEwen, B.S., 1998. Stress, adaptation, and disease: allostasis and allostatic load. Ann. N. Y. Acad. Sci. 840 (1), 33–44. https://doi.org/10.1111/j.1749-6632.1998.tb09546.x.

McEwen, B.S., 2007. Physiology and neurobiology of stress and adaptation: central role of the brain. Physiol. Rev. 87 (3), 873–904. https://doi.org/10.1152/physrev.00041.2006.

McEwen, B.S., Gianaros, P.J., 2011. Stress- and allostasis-induced brain plasticity. Annu. Rev. Med. 62 (1), 431–445. https://doi.org/10.1146/annurev-med-052209-100430.

Meer, J.N.V.D., Breakspear, M., Chang, L.J., Sonkusare, S., Cocchi, L., 2020. Movie viewing elicits rich and reliable brain state dynamics. Nat. Commun. 11 (1), 5004. https://doi.org/10.1038/s41467-020-18717-w.

Noack, H., Nolte, L., Nieratschker, V., Habel, U., Derntl, B., 2019. Imaging stress: an overview of stress induction methods in the MR scanner. J. Neural Transm. 126 (9), 1187–1202. https://doi.org/10.1007/s00702-018-01965-y.

Parkes, L., Fulcher, B., Yücel, M., Fornito, A., 2018. An evaluation of the efficacy, reliability, and sensitivity of motion correction strategies for resting-state functional MRI. Neuroimage 171, 415–436. https://doi.org/10.1016/j.neuroimage.2017.12.073.

Raichle, M.E., MacLeod, A.M., Snyder, A.Z., Powers, W.J., Gusnard, D.A., Shulman, G.L., 2001. A default mode of brain function. Proceed. Nat. Acad. Sci. 98 (2), 676–682. https://doi.org/10.1073/pnas.98.2.676.

Ren, X., Zhao, X., Li, J., Liu, Y., Ren, Y., Pruessner, J.C., Yang, J., 2022. The hippocampal–Ventral medial prefrontal cortex neurocircuitry involvement in the association of daily life stress with acute perceived stress and cortisol responses. Psychosom. Med. 84 (3), 276–287. https://doi.org/10.1097/PSY.0000000000001058.

Reynaud, E., Guedj, E., Souville, M., Trousselard, M., Zendjidjian, X., El Khoury-Malhame, M., Fakra, E., Nazarian, B., Blin, O., Canini, F., Khalfa, S., 2013. Relationship between emotional experience and resilience: an fMRI study in fire-fighters. Neuropsychologia 51 (5), 845–849. https://doi.org/10.1016/j.neuropsychologia.2013.01.007.

Shalev, A., Liberzon, I., Marmar, C., 2017. Post-traumatic stress disorder. New England J. Med. 376 (25), 2459–2469. https://doi.org/10.1056/NEJMra1612499.

Sharma, R., Smith, S.A., Boukina, N., Dordari, A., Mistry, A., Taylor, B.C., Felix, N., Cameron, A., Fang, Z., Smith, A., Ismail, N., 2020. Use of the birth control pill affects stress reactivity and brain structure and function. Horm. Behav. 124, 104783. https://doi.org/10.1016/j.yhbeh.2020.104783.

Shirer, W.R., Ryali, S., Rykhlevskaia, E., Menon, V., Greicius, M.D., 2012. Decoding subject-driven cognitive states with whole-brain connectivity patterns. Cerebral Cortex 22 (1), 158–165. https://doi.org/10.1093/cercor/bhr099.

Stange, J.P., Alloy, L.B., Fresco, D.M., 2017. Inflexibility as a vulnerability to depression: a systematic qualitative review. Clinical Psychol.: Sci. Practice 24 (3), 245–276. https://doi.org/10.1111/cpsp.12201.

Stevner, A.B.A., Vidaurre, D., Cabral, J., Rapuano, K., Nielsen, S.F.V., Tagliazucchi, E., Laufs, H., Vuust, P., Deco, G., Woolrich, M.W., Van Someren, E., Kringelbach, M.L., 2019. Discovery of key whole-brain transitions and dynamics during human wakefulness and non-REM sleep. Nat. Commun. 10 (1), 1035. https://doi.org/10.1038/s41467-019-08934-3.

Streit, F., Haddad, L., Paul, T., Frank, J., Schäfer, A., Nikitopoulos, J., Akdeniz, C., Lederbogen, F., Treutlein, J., Witt, S., Meyer-Lindenberg, A., Rietschel, M., Kirsch, P., Wüst, S., 2014. A functional variant in the neuropeptide S receptor 1 gene moderates the influence of urban upbringing on stress processing in the amygdala. Stress. 17 (4), 352–361. https://doi.org/10.3109/10253890.2014.921903.

Tobia, M.J., Hayashi, K., Ballard, G., Gotlib, I.H., Waugh, C.E., 2017. Dynamic functional connectivity and individual differences in emotions during social stress. Hum. Brain Mapp. 38 (12), 6185–6205. https://doi.org/10.1002/hbm.23821.

Toffoletto, S., Lanzenberger, R., Gingnell, M., Sundström-Poromaa, I., Comasco, E., 2014. Emotional and cognitive functional imaging of estrogen and progesterone effects in the female human brain: a systematic review. Psychoneuroendocrinology. 50, 28–52. https://doi.org/10.1016/j.psyneuen.2014.07.025.

Vaisvaser, S., Lin, T., Admon, R., Podlipsky, I., Greenman, Y., Stern, N., Fruchter, E., Wald, I., Pine, D.S., Tarrasch, R., Bar-Haim, Y., Hendler, T., 2013. Neural traces of stress: cortisol related sustained enhancement of amygdala-hippocampal functional connectivity. Front. Hum. Neurosci. 7. https://doi.org/10.3389/fnhum.2013.00313.

van der Maaten, L., Hinton, G., 2008. Visualizing data using t-SNE. J. Machine Learn. Res. 9, 2579–2605. WOS:000262637600007.

Van Oort, J., Tendolkar, I., Hermans, E.J., Mulders, P.C., Beckmann, C.F., Schene, A.H., Fernández, G., Van Eijndhoven, P.F., 2017. How the brain connects in response to acute stress: a review at the human brain systems level. Neurosci. Biobehav. Rev. 83, 281–297. https://doi.org/10.1016/j.neubiorev.2017.10.015.

Veer, I.M., Oei, N.Y.L., Spinhoven, P., Van Buchem, M.A., Elzinga, B.M., Rombouts, S.A. R.B., 2011. Beyond acute social stress: increased functional connectivity between amygdala and cortical midline structures. Neuroimage 57 (4), 1534–1541. https://doi.org/10.1016/j.neuroimage.2011.05.074.

Vidaurre, D., Llera, A., Smith, S.M., Woolrich, M.W., 2021. Behavioural relevance of spontaneous, transient brain network interactions in fMRI. Neuroimage 229, 117713. https://doi.org/10.1016/j.neuroimage.2020.117713.

Vidaurre, D., Quinn, A.J., Baker, A.P., Dupret, D., Tejero-Cantero, A., Woolrich, M.W., 2016. Spectrally resolved fast transient brain states in electrophysiological data. Neuroimage 126, 81–95. https://doi.org/10.1016/j.neuroimage.2015.11.047.

Vidaurre, D., Smith, S.M., Woolrich, M.W., 2017. Brain network dynamics are hierarchically organized in time. Proceed. Nat. Acad. Sci. 114 (48), 12827–12832. https://doi.org/10.1073/pnas.1705120114.

Yan, C.-G., Wang, X.-D., Zuo, X.-N., Zang, Y.-F., 2016. DPABI: data processing & analysis for (Resting-State) Brain imaging. Neuroinformatics. 14 (3), 339–351. https://doi.org/10.1007/s12021-016-9299-4.

Yarkoni, T., Poldrack, R.A., Nichols, T.E., Van Essen, D.C., Wager, T.D., 2011. Large-scale automated synthesis of human functional neuroimaging data. Nat. Methods 8 (8), 665–670. https://doi.org/10.1038/nmeth.1635.

Zeng, Y., Xiong, B., Gao, H., Liu, C., Chen, C., Wu, J., Qin, S., 2024. Cortisol awakening response prompts dynamic reconfiguration of brain networks in emotional and executive functioning. Proceed. Nat. Acad. Sci. 121 (52), e2405850121. https://doi.org/10.1073/pnas.2405850121.

Zhang, W., Hashemi, M.M., Kaldewaij, R., Koch, S.B.J., Beckmann, C., Klumpers, F., Roelofs, K., 2019. Acute stress alters the 'default' brain processing. Neuroimage 189, 870–877. https://doi.org/10.1016/j.neuroimage.2019.01.063.

Zhang, W., Kaldewaij, R., Hashemi, M.M., Koch, S.B.J., Smit, A., Van Ast, V.A., Beckmann, C.F., Klumpers, F., Roelofs, K., 2022. Acute-stress-induced change in salience network coupling prospectively predicts post-trauma symptom development. Transl. Psychiatry 12 (1), 63. https://doi.org/10.1038/s41398-022-01798-0.

Zhang, W., Llera, A., Hashemi, M.M., Kaldewaij, R., Koch, S.B.J., Beckmann, C.F., Klumpers, F., Roelofs, K., 2020. Discriminating stress from rest based on resting-state connectivity of the human brain: a supervised machine learning study. Hum. Brain Mapp. 41 (11), 3089–3099. https://doi.org/10.1002/hbm.25000.